Journal of Magnetic Resonance **149,** 119–125 (2001)
doi:10.1006/jmre.2000.2280, available online at http://www.idealibrary.com on IDEAL®

Two-Voxel Localization Sequence for *in Vivo* Two-Dimensional Homonuclear Correlation Spectroscopy[1]

Florence Delmas,*,† Jean-Claude Beloeil,* Boudewijn P. J. van der Sanden,† Klaas Nicolay,† and Brigitte Gillet*

*Laboratoire de RMN Biologique, ICSN-CNRS, 91198 Gif sur Yvette, France; and †Department of Experimental in vivo NMR, Image Science Institute, University Medical Center, Utrecht, The Netherlands

Received August 7, 2000; revised December 7, 2000

The combination of localized 2D ^{1}H MR correlation spectroscopy and Hadamard encoding allows the simultaneous acquisition of multiple volumes of interest without an increase in the experimental duration, compared to single-voxel acquisition. In the present study, 2D correlation spectra were acquired simultaneously within 20 to 40 min in two voxels located in each hemisphere of the rat brain. An intervoxel distance of 20% of the voxel size was sufficient to limit spatial contamination. The following cerebral metabolites gave detectable crosspeaks: *N*-acetylaspartate, the glutamate/glutamine pool, aspartate, phosphoethanolamine, glucose, glutathione, taurine, *myo*-inositols, lactate, threonine, γ-aminobutyric acid, and alanine. Most of the metabolites were measured without contamination of other resonances.

Key Words: **two-dimensional correlation ^{1}H MRS; multivoxel localization; Hadamard encoding; rat brain; cerebral metabolites.**

INTRODUCTION

Localized *in vivo* ^{1}H magnetic resonance spectroscopy (MRS) has proven to be a useful tool for the study of the brain in normal and pathophysiological conditions. *N*-Acetylaspartate (NAA), which gives the largest peak in 1D spectra of the normal brain, has been extensively used as a marker of neuronal dysfunction (*1*). Under ischemic–hypoxic conditions, lactate—the end product of anaerobic glycolysis—increases, which gives rise to another prominent peak in 1D ^{1}H MR spectra. This has been explored in numerous studies (*2*). Up to 35 cerebral metabolites that can be detected by ^{1}H MRS were recently reviewed by Govindaraju *et al.* (*3*). Most of them have received little attention, since their detection is very challenging.

One-dimensional ^{1}H MR spectra of the brain are associated with low spectral dispersion at field strengths commonly used for *in vivo* studies. The main resonances are restricted to a narrow chemical shift range of 5 ppm. Detection of most metabolites is hampered by spectral overlap with other metabolites, the broad water resonance, or the macromolecular background, as well as low concentration and/or multiplet splitting. The observation of a large number of resonances requires high field strength (9.4 T) and very short echo time, as demonstrated by Pfeuffer *et al.* (*4*), who were able to assign and quantify 18 metabolites in 1D ^{1}H MR spectra of the rat brain. At lower field strength, spectral editing techniques may be required for the detection of poorly accessible metabolites such as γ-aminobutyric acid (*5*), as well as for the unambiguous detection of resonances that may suffer from strong overlap such as lactate (*6, 7*). However, these techniques are optimized for a particular spin system and are not adapted to the simultaneous detection of a large number of metabolites.

The problem of spectral overlap can be overcome by the use of two-dimensional correlation spectroscopy (*8, 9*), even at low field strength (*10, 11*), as resonances are spread on a two-dimensional surface. Localized *in vivo* 2D ^{1}H MRS allows separation of most overlapping peaks for coupled spin systems that give rise to off-diagonal peaks. For instance, the singlet resonance of the methyl group of NAA (2.01 ppm) observed in 1D ^{1}H MRS is overlapped by the resonances of the glutamate/glutamine pool (2.08/2.12 ppm), γ-aminobutyric acid (1.89 ppm), and *N*-acetylaspartatylglutamate (2.05 ppm). In 2D correlation spectra, this NAA singlet at 2.01 ppm appears on the diagonal and protons from the aspartate moiety give rise to an off-diagonal peak, not contaminated by other resonances. Furthermore, the AX_3 spin system of lactate gives rise to a correlation peak, free of any contribution from lipids. Localized *in vivo* 2D ^{1}H MRS also gives access to coupled spin systems with complicated coupling patterns such as the glutamate/glutamine pool and γ-aminobutyric acid, which are more difficult to observe by 1D ^{1}H MRS. Finally, the measurement of less concentrated metabolites (concentration <3 μmol/g, (*4*)) such as aspartate, alanine, phosphoethanolamine, and glucose is facilitated, as dispersion is enhanced.

In previous *in vivo* rat brain studies, multivoxel localization of 2D spectra has been obtained in two spatial dimensions (*12*) by combining ^{1}H MRSI (*13*) and a COSY sequence (*14*). This sequence was applied to measure the steady-state metabolism of primary brain tumors within 3 h. Valuable information on the spatial distribution of several metabolites was recorded.

[1] This study was sponsored in part by the French Ministry of Research and Technology, Grant 97555. Financial support from the SONNMR Large-Scale Facility is acknowledged.

1090-7807/01 $35.00

However, this method cannot be used for dynamic studies of metabolic changes. When a small number of voxels is sufficient to cover the region of interest (maximum of 8 in each spatial dimension), another less time-consuming technique—Hadamard encoding—is more convenient. In Hadamard-encoded experiments, phase-encoding RF pulses are used for spatial encoding (*15*), instead of the phase-encoding gradients used in ^{1}H MRSI methods. In comparison to ^{1}H MRSI, the number of Hadamard-encoded voxels is limited, due to pulse power requirements. However, Hadamard encoding is less prone to voxel bleeding, which is a problem when a small numbers of phase encoding steps is used (*16*). Thus, Hadamard encoding is more appropriate for the simultaneous acquisition of a limited number of voxels. Hadamard spectroscopic imaging (HSI) has previously been applied to 1D spectroscopy (*17*) and has been combined with ^{1}H MRSI (*18–20*).

The aim of this study was to develop a two-voxel localization sequence for 2D ^{1}H MR correlation spectroscopy for *in vivo* applications in rat brain to measure cerebral metabolites without spectral contamination. The single-voxel localized 2D ^{1}H MRS sequence (*21*) was modified to allow simultaneous refocusing of two frequency bands. Since no extra time was required for the spatial encoding, the total acquisition time was identical to a single-voxel experiment. This two-voxel localized 2D ^{1}H MRS sequence is suited to the study of metabolic alterations that only affect one cerebral hemisphere, such as focal cerebral ischemia or brain tumors. In the present study, two spectra were simultaneously acquired in normal and global ischemic rat brain. Similarity of the spectra from the two hemispheres will indicate that the spectra of the contralateral voxel can be used as a reference in studies of focal brain damage.

RESULTS AND DISCUSSION

In this section, first the two-voxel 2D ^{1}H MRS sequence will be explained in detail. Second, results of an *in vitro* study on a two-compartment model will be presented. Finally, the localization properties of the sequence and spectroscopy results will be illustrated *in vivo* on a rat brain. All experiments were acquired on a Varian imaging spectrometer interfaced to a 4.7-T Oxford magnet equipped with a 12-cm high-performance gradient insert (220 mT/m in 300 μs). Signal excitation was performed by a Helmholtz coil actively decoupled from a 25-mm surface coil used for signal reception.

Two-Voxel 2D ^{1}H MR Spectroscopy

Three slice-selective RF pulses were used in a double-spin-echo volume selective sequence (*22*) (see Fig. 1). A pure phase pulse (eburp 1) was used for excitation (*23*). This pulse does not induce dephasing through the slice; therefore, refocusing after the application of the first slice-selective gradient was not required. The final pulse was a hermitian 90° pulse, which was applied for 2D polarization transfer.

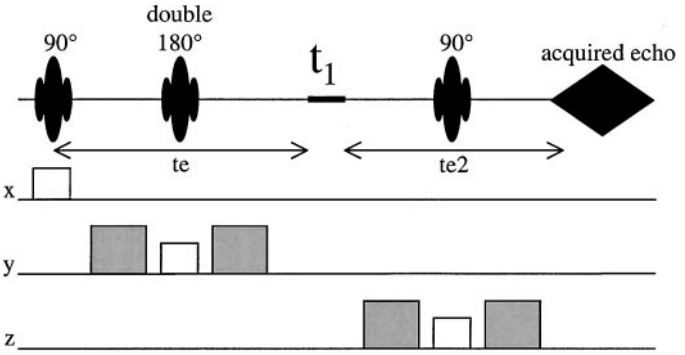

FIG. 1. Two-voxel 2D ^{1}H MRS sequence. This sequence must be applied twice with two different double 180° refocusing pulses to perform spatial encoding in the *y* direction. The slice selection gradients are shown in white and the crusher gradients in gray. See text for description of the sequence.

Hadamard encoding was performed with a double 180° refocusing pulse. Although any of the pulses can theoretically be used for encoding, the 180° was chosen since better slice profiles were obtained with this pulse. An optimized sinc pulse (*24*) was modified to allow double refocusing. The pulses were generated with homemade software (kindly provided by Dr. R. A. de Graaf, MRC, Yale University, New Haven, CT). The superposition principle developed by Müller (*25*) was used for the generation of the double refocusing pulses. These multiband RF pulses can be applied for closely spaced bands. A gap of 10–20% of the voxel size is nevertheless recommended unless pulses with improved multiband excitation profiles are used (Shinnar–Le Roux method (*26*)). The acquisition was performed in two steps, since two different pulses are required for encoding. The first pulse induces equal phases in the two simultaneously refocused slices, and the second one induces opposite phases. Postacquisition decoding was obtained by addition and subtraction of the two Hadamard-encoded spectra, which corresponds to the multiplication of the data by the Hadamard matrix. The echo times TE and TE2 were kept to minimum values of 7.65 and 4.85 ms, respectively (Fig. 1). The second dimension was obtained by increasing the t_1 delay. Fourier transformation was applied in both dimensions resulting in a COSY-type spectrum.

Water suppression (not represented in Fig. 1) was obtained using three gaussian CHESS pulses followed by crusher gradients. The third CHESS pulse was optimized to yield $M_z = 0$ for water at the start of the localization sequence, i.e., to account for T_1 relaxation during the last crusher gradient (*27*). Efficient water suppression is of great importance for multivoxel experiments such as ^{1}H MRSI and HSI since a relatively broad water peak has to be suppressed. Linewidths are larger than those obtained from single-voxel experiments, where measurements in smaller and more homogeneous volumes are usually performed.

This multiple excitation technique encounters the same chemical shift misregistration problem as single-voxel methods (*28*).

The misregistration in each spatial dimension depends on the bandwidth of the corresponding slice-selective pulse. This problem can easily be minimized by using large bandwidths for all three selective pulses. Therefore, bandwidths of 3000 Hz were employed, corresponding to a chemical shift dependence of ~0.33 mm/ppm.

Phantom Experiments

The sequence was tested on a phantom made of two cylinders. A 1-cm-diameter tube filled with a 100 mM solution of γ-aminobutyric acid was placed inside a 3-cm-diameter tube filled with a 100 mM lactate solution. One of the voxels was positioned in the tube containing the γ-aminobutyric acid solution and the other one in the tube containing the lactate solution. The results are shown in Fig. 2.

The extracted spectra show very little contamination, which indicates the good performance of the double refocusing pulse (Figs. 2C and 2D). The minor lactate contamination visible in Fig. 2D probably arises from the nonperfect slice profile of the excitation pulse in the *x* direction, since no spoiling gradients are used in the *x* direction. The level of contamination is below 2%, which is the ratio of integrals of the diagonal peaks at 1.3 ppm in Figs. 2C and 2D. This can be neglected in *in vivo* experiments, where lower metabolite concentrations are found.

An interesting feature of Hadamard encoding is that any region of interest in the field of view can be sampled without causing folding-over problems. The two voxels are situated along the *y* direction, with common *x* and *z* coordinates. The distance between the two voxels can be chosen at will. This configuration is especially appropriate when a symmetrical structure such as the brain is studied.

In Vivo Experiments

2D ^{1}H MR correlation spectroscopy was performed *in vivo* after image-guided positioning of a voxel in each cerebral hemisphere of a rat, as depicted in Fig. 3A. Acquisition parameters for the 2D spectra were carefully chosen in such a way that maximum signal intensity was obtained for the crosspeaks

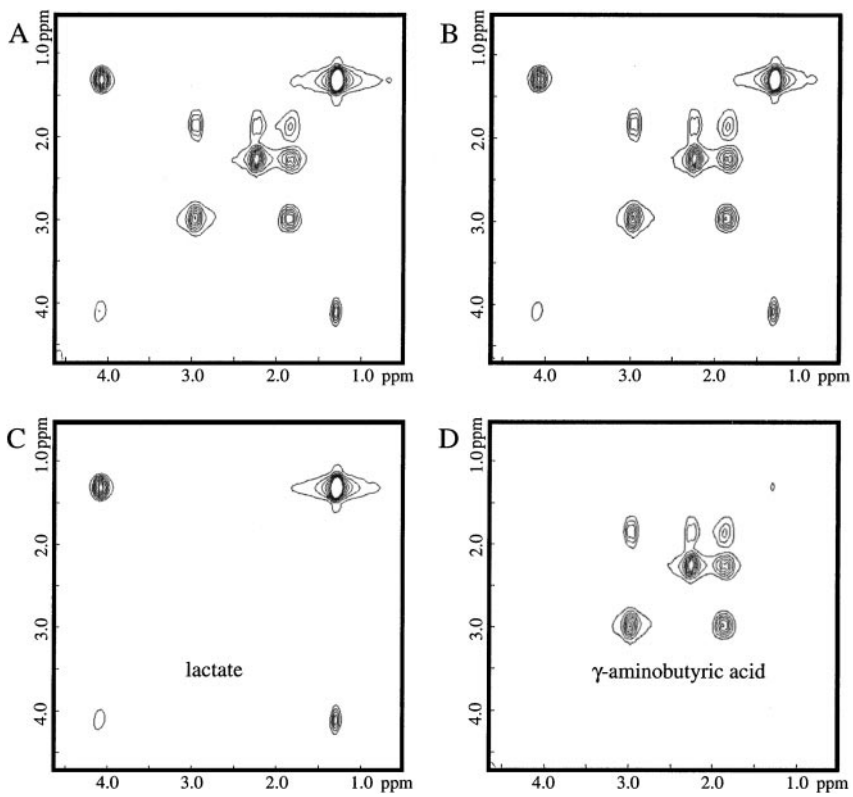

FIG. 2. 2D correlation spectra of a two-compartment phantom made of two tubes containing solutions of γ-aminobutyric acid and lactate, before and after multiplication by the Hadamard matrix. In the first spectral dimension ($t2$), 1024 points were acquired. In the second spectral dimension ($t1$), 64 increments were acquired corresponding to a t_1-window of 32 ms, with an initial t_1 value of 15 ms. The spectral width was 2000 Hz in both dimensions. Four scans were accumulated for each t_1 increment. Repetition time was 2 s and the voxel size was 125 μl. A–B: Hadamard-encoded spectra corresponding to (A) equivalent and (B) opposite phases in the two refocused slices. C–D: Extracted spectra corresponding to the two encoded voxels. Data postprocessing, including Hadamard-decoding, was performed with GIFA software (ftp://www.cbs.univ-montp1.fr/pub/gifa_v4). The 2D data set was apodized with a standard sine function and zero filled in both dimensions.

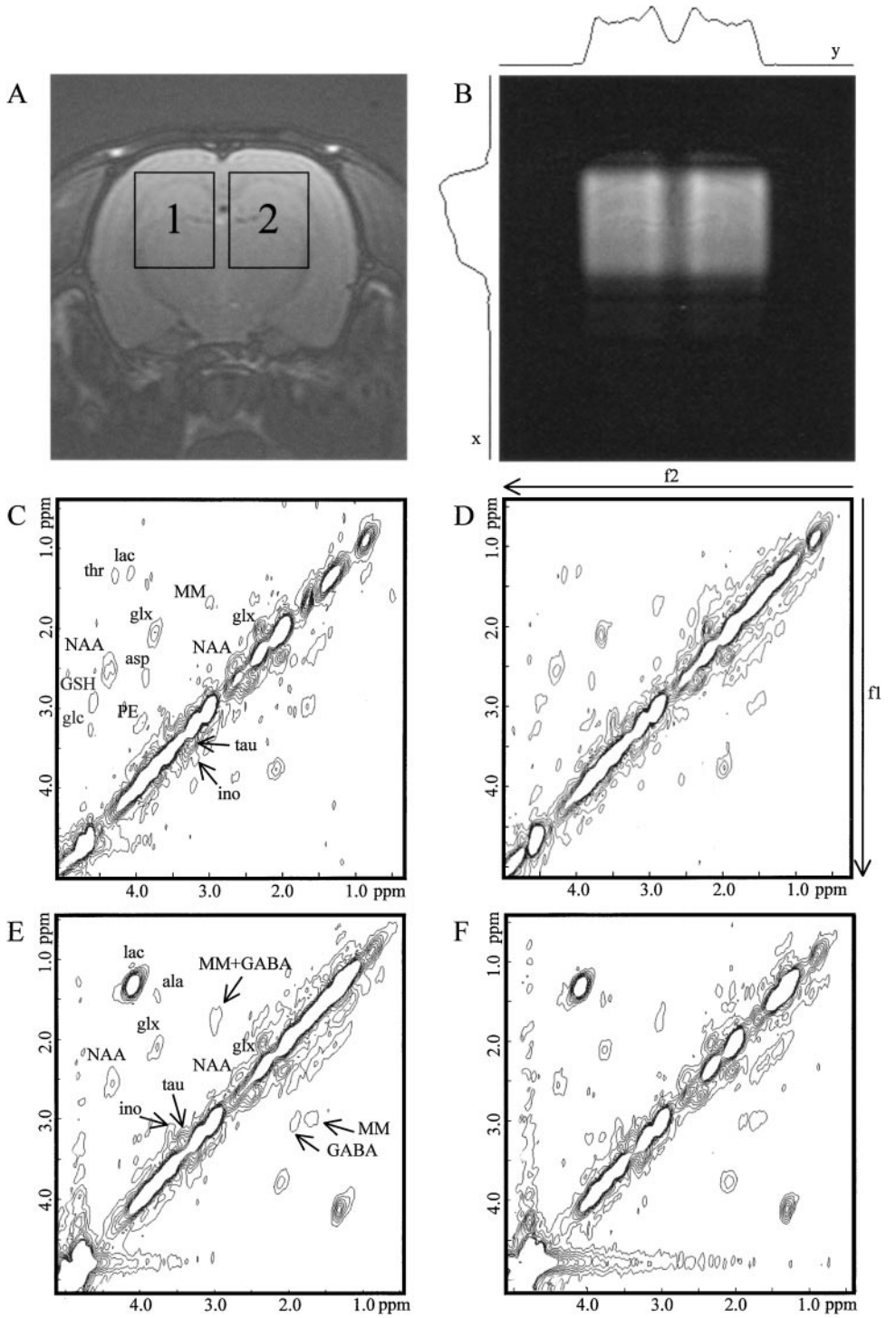

FIG. 3. *In vivo* multivoxel 2D spectroscopy: image-guided positioning of the voxels and associated spectra in the normal and ischemic rat brain. Adult male Wistar rats were anesthetized with 0.8% halothane in N_2O/O_2 (7 : 3). The tidal CO_2 was continuously monitored and maintained within physiological boundaries. Body temperature was kept at ~37°C using a warm blanket with a feedback system. The repetition time was triggered by the breathing pace of about 2 s. A: MR image of transversal slice through the rat brain showing the position of the two voxels. B: MR image of the localized volume selected by the multivoxel 2D experiment with projections in the *x* and *y* directions. C–F: Localized 2D ^{1}H MR spectra after decoding. The spectral width was 2000 Hz in both dimensions. In the first spectral dimension ($t2$), 512 points were acquired. In the second spectral dimension ($t1$), 80 increments were acquired corresponding to a t_1-window of 40 ms, with an initial t_1 value of 15 ms. Eight scans were accumulated for each t_1 increment. Repetition time was 2 s and the voxel size was 125 μl. Total acquisition time for each Hadamard-encoded experiment was 21 min. C–D: Spectra corresponding to voxels 1 (C) and 2 (D) of a normal rat brain. E–F: Spectra originating from the same voxels immediately after global ischemia induced by cardiac arrest. For peaks attributions, see Table 1. Data postprocessing, including Hadamard-decoding, was performed with GIFA software (ftp://www.cbs.univ-montp1.fr/pub/gifa_v4). The 2D data set was apodized with a standard sine function and zero filled in both dimensions.

of the different cerebral metabolites. Of great importance is the choice of the sampling period in the second spectral dimension (t_1-window), which has to be adapted to the different spin systems of the metabolites (*29*). Three parameters determining the t_1-window have to be optimized, namely the initial t_1 value, the step size (t_1-increment), and the number of steps (see comments on Figs. 3C–3F). Mutual interactions of the spins in each different spin system give rise to specific t_1-dependence and a large variety of spin systems must be taken into account, such as the ABX system of *N*-acetylaspartate (with two strongly coupled methylene protons at 4.7 T), the AMNPQ system of glutamate, or the AX_3 system of lactate.

Satisfactory localization is obtained *in vivo* (Fig. 3B), and only minor contamination is observed in the Hadamard-encoded direction, resulting from the nonperfect slice edge definition, as illustrated by the projection in the *y* direction in Fig. 3B. It must be stressed that these profiles correspond to uncoupled spin systems. In cases of coupled spin systems, the profile can be distorted as shown by Reddy *et al.* (*30*). In the normal rat brain (Figs. 3C and 3D), crosspeaks were assigned to *N*-acetylaspartate, the glutamate/glutamine pool (glx), aspartate (asp), phosphoethanolamine (PE), glucose (glc), glutathione (GSH), lactate (lac), and threonine (thr). The crosspeaks of *N*-acetylaspartate and the glutamate/glutamine pool show good signal-to-noise ratio consistent with higher concentrations compared to other metabolites (*4*). In the ischemic rat brain (Figs. 3E and 3F), the main crosspeaks were assigned to *N*-acetylaspartate, the glutamate/glutamine pool, and lactate. Less concentrated metabolites such as γ-aminobutyric acid (GABA) and alanine (ala) also appeared. Chemical shifts of the observed crosspeaks are presented in Table 1. In both ischemic and normal rat brain, clear detection of the crosspeaks of taurine and *myo*-inositols requires the application of a different apodization function, since they are situated close to the diagonal (see Table 1). Optimized water suppression enabled the observation of peaks with $f2$ coordinates close to the water resonance (4.78 ppm). Linewidths of $\sim$14 Hz at half maximum were measured for the unsuppressed water peak in the normal brain. After global ischemia, the water linewidth increased, resulting in less effective water suppression.

Comparison of spectra in the normal and ischemic rat brain shows changes in metabolite levels. The linear relationship between crosspeak volume and concentration has been previously shown (*31*). Quantification of these concentration changes would require measurements of changes in T_2 values of the different metabolites.

Compared to the normal rat brain spectra, the ischemic brain spectra show a clear increase in the detected levels of lactate, alanine, and γ-aminobutyric acid and a decrease in the detected levels of *N*-acetylaspartate, aspartate, glucose, and glutathione. The similarity of the spectra arising from the two hemispheres in both normal and ischemic brain shows the reproducibility of the measurement. The sequence is therefore suited to analyzing metabolic changes located in a cerebral hemisphere and simultaneously recording ipsilateral and contralateral spectra.

TABLE 1
Assignments of Off-Diagonal Peaks in the Upper Triangle

Metabolite	Crosspeaks origin	$f1$ coordinate (ppm)	$f2$ coordinate (ppm)
N-Acetylaspartate (NAA)	CH_2 ($\beta\beta'$)–CH (α)	2.6	4.4
	CH_2 ($\beta\beta'$)	2.5	2.7
Alanine (ala)	CH_3 (β)–CH (α)	1.5	3.8
γ-Aminobutyric acid (GABA)	CH_2 (β)–CH_2 (γ)	1.9	3.0
	CH_2 (β)–CH_2 (α)	1.9	2.3
Aspartate (asp)	CH_2 ($\beta\beta'$)–CH (α)	2.7	3.9
Glucose (β anomer) (glc)	H_2–H_1	3.2	4.6
Glutamate/glutamine pool (glx)	CH_2 (β)[a]–CH(α)	2.1	3.7/3.75
	CH_2 (β)[a]–CH (γ)	2.1	2.3/2.4
Glutathione (cysteine moiety) (GSH)	CH_2–CH	2.95	4.6
myo-Inositols (ino)	H_5–H_4, H_6	3.3	3.6
Lactate (lac)	CH_3 (β)–CH (α)	1.3	4.1
Phosphoethanolamine (PE)	CH_2–CH_2	3.2	4.0
Taurine (tau)	SCH_2–NCH_2	3.25	3.4
Threonine (thr)	CH_3 (γ)–CH (β)	1.3	4.25

Note. Symmetric chemical shifts can be deduced for the lower triangle.
[a] The two methylene protons (β protons) are equivalent in the glutamine molecule but not in the glutamate molecule.

Asymmetric spectra are obtained with regard to the diagonal (*8*). In the case of two coupled protons A and X, the coherence transfer signal between A and X situated on one side of the diagonal is proportional to the magnetization of A, whereas the coherence transfer signal between X and A situated on the other side is proportional to the magnetization of X. Because of this asymmetry, the effect of water suppression on neighboring crosspeaks depends on the proton at the origin of the polarization transfer. For instance, the NAA crosspeak originating from the resonance at 4.4 ppm (lower triangle) is suppressed together with the water peak, whereas the crosspeak originating from the resonances at 2.5/2.7 ppm (upper triangle) shows no signal loss (Figs. 3C–3F).

Despite the improvement in spectral dispersion in the 2D maps, overlap is still present in a limited number of cases. One of the main sources of overlap in 2D spectra can be the presence of identical entities in molecules, such as amino acid entities (i.e., glutamate and aspartate). In the normal rat brain, only the glutamate moiety of glutathione (2.15/3.77 ppm) and glutamate (2.08/3.77 ppm) suffers from such an overlap. In the ischemic rat brain, a different type of superposition is observed. The lactate crosspeak (1.31/4.10 ppm), although free of any contribution from methylene groups of lipids, overlaps the threonine crosspeak (1.32/4.25 ppm) (see Figs. 3C and 3D). The main reason

for this is the broadening of the lactate peak, which could originate from binding effects (*32*). In the case of high lactate levels, the situation is aggravated.

Both normal and ischemic brain show a single strong contribution from the macromolecular background (see MM on Figs. 3C–3F). This result is in agreement with nonlocalized 2D experiments carried out by Behar and Ogino (*33*). In the ischemic rat brain, this macromolecular resonance hampers the observation of the γ-aminobutyric acid crosspeaks at 1.9 ppm ($f1$)/3.0 ppm ($f2$), since the two peaks are not resolved. However, observation at 3.0 ppm ($f1$)/1.9 ppm ($f2$) is possible (see Figs. 3E and 3F).

Compared to 1D spectroscopy, 2D spectroscopy allowed the detection of more metabolites. The observation of the glutamate/glutamine pool level was highly facilitated. However, possible contamination from the glutamate part of glutathione is not excluded. Metabolites with very low concentrations such as alanine, γ-aminobutyric acid, aspartate, glucose, glutathione, phosphoethanolamine, and threonine were detected. *N*-Acetylaspartate could be measured without contamination. The lactate peak in the hypoxic–ischemic rat brain spectra was separated from lipids or macromolecular contribution, but could not be separated from the threonine peak.

Absolute quantification of the different metabolites was beyond the scope of this study; however, the acquisition of "noncontaminated" data is valuable for the assessment of metabolite levels and their time course evolution during a pathophysiological process. This technique will be applied in particular to study metabolic changes after the onset of focal cerebral ischemia in rats, but it is also applicable to studying metabolic changes in brain tumors.

Temporal resolution was, together with dispersion enhancement, one of the major issues of this study. Total acquisition time for the spectra in Figs. 3C–3F was 42 min. However, an acquisition of 21 min was possible for the detection of the most concentrated metabolites such as *N*-acetylaspartate or glutamate/glutamine. Metabolites at lower concentrations, such as aspartate (*4*), were still observable but at the limit of detection. Importantly, in Hadamard-encoded experiments, the minimum time required for the acquisition of a single-voxel spectrum is used efficiently for spatial encoding (*17*). When n accumulations per t_1-increment are necessary for a two-voxel experiment, each of the two experiments required for encoding are run with $n/2$ accumulations. After decoding, this results in the equivalent of n accumulations for each voxel, with no penalty in experimental duration compared to a single-voxel acquisition. In general, a $\sqrt{N}$-fold gain in sensitivity is obtained for N encoded voxels (*34*). The amount of time that was spent for the two-voxel experiment could also be used to encode a higher number of spatial locations using a four-band or an eight-band refocusing pulse. If the same total volume was encoded with a higher number of voxels, the experimental duration would be determined by the signal-to-noise ratio, and not by the spatial encoding procedure.

The use of smaller voxels requires improvement of the signal-to-noise ratio for some of the observed metabolites. The signal-to-noise ratio can be improved by using matched filtering in t_2 and by apodizing the signal in t_1 during acquisition (*29*). This will allow the use of smaller voxels without any information loss.

CONCLUSION

It was shown that multivoxel 2D ^{1}H MR correlation spectroscopy can be applied *in vivo* in the rat brain with a favorable temporal resolution. Two-volume localization was obtained, with limited signal bleeding, using Hadamard encoding, as shown on a two-compartment phantom. This method is preferable to phase-encoding methods (^{1}H MRSI) when matrices of limited size are sampled. The gain in spectral resolution, in comparison to one-dimensional spectroscopy, gives access to a larger number of cerebral metabolites. Detection of resonances without contamination of other resonances is possible for most correlation peaks recorded.

ACKNOWLEDGMENTS

The authors thank Dr. R. A. de Graaf for advice and for providing the double-slice refocusing pulses. They also thank W. Veldhuis and Dr. E. Blezer for biotechnical assistance and Gerard van Vliet for expert technical assistance. This study was performed at the SONNMR Large-Scale Facility for Biomolecular NMR that is supported by the EU-Program for Access to Research Infrastructure.

REFERENCES

1. G. Tsai and J. T. Coyle, *N*-Acetylaspartate in neuropsychiatric disorders, *Prog. Neurobiol.* **46,** 531–540 (1995).
2. J. W. Prichard, What the clinician can learn from MRS lactate measurements, *NMR Biomed.* **4,** 99–102 (1991).
3. V. Govindaraju, K. Young, and A. A. Maudsley, Proton NMR chemical shifts and coupling constants for brain metabolites, *NMR Biomed.* **13,** 129–153 (2000), doi: 10.1002/jmre.1099.1492.
4. J. Pfeuffer, I. Tkác, S. W. Provencher, and R. Gruetter, Towards an *in vivo* neurochemical profile: Quantification of 18 metabolites in short-echo-time ^{1}H NMR spectra of the rat brain, *J. Magn. Reson.* **141,** 104–120 (1999), doi: 10.1006/jmre.1999.1895.
5. J. R. Keltner, L. L. Wald, B. de B. Frederick, and P. F. Renshaw, *in vivo* detection of GABA in human brain using a localized double quantum filter technique, *Magn. Reson. Med.* **37,** 366–371 (1997).
6. R. A. de Graaf, Y. Luo, M. Terpstra, and M. Garwood, Spectral editing with adiabatic pulses, *J. Magn. Reson.* B**109,** 184–193 (1995).
7. R. E. Hurd and D. Freeman, Proton editing and imaging of lactate, *NMR Biomed.* **4,** 73–80 (1991).
8. B. Gillet, P. Meric, and J.-C. Beloeil, Two-dimensional NMR spectroscopy for studies on animal models of cerebral metabolism, *J. Magn. Reson. Anal.* **2,** 103–109 (1996).
9. S. Brulatout, P. Meric, I. Lubinoux, J. Borredon, J.-L. Correze, P. Roucher, B. Gillet, G. Berenger, J.-C. Beloeil, B. Tiffon, J. Mispelter, and J. Seylaz, 1D (proton and phosphorus) and 2D (proton) *in vivo* NMR spectroscopy study of reversible global cerebral ischemia, *J. Neurochem.* **66,** 2491–2499 (1996).

10. B. Gillet, A. Ziegler, J.-F. Nedelec, J.-P. Macher, J.-C. Beloeil, and M. Décorps, Localized 2D correlation spectroscopy in human brain at 3T, ESMRMB, Seville, 1999, Abstract 548.
11. L. N. Ryner, J. A. Sorenson, and M. A. Thomas, 3D localized 2D NMR spectroscopy on an MRI scanner, *J. Magn. Reson.* B**107,** 126–137 (1995).
12. M. von Kienlin, A. Ziegler, Y. Le Fur, C. Rubin, M. Décorps, and C. Rémy, 2D-spatial/2D-spectral spectroscopic imaging of intracerebral gliomas in rat brain, *Magn. Reson. Med.* **43,** 211–219 (2000).
13. T. R. Brown, B. M. Kincaid, and C. Ugurbil, NMR chemical shift imaging in three dimensions, *Proc. Natl. Acad. Sci. USA* **79,** 3523 (1982).
14. J. Jeener, unpublished lecture, Ampere International Summer School, Basko Polje, Yugoslavia, 1971.
15. J. Hennig, Chemical shift imaging with phase encoding RF pulses, *Magn. Reson. Med.* **25,** 289–298 (1992).
16. T. R. Brown, Practical applications of chemical shift imaging, *NMR Biomed.* **5,** 238–243 (1992).
17. L. Bolinger and J. S. Leigh, Hadamard spectroscopic imaging (HIS) for multivolume localization, *J. Magn. Reson.* **80,** 162–167 (1988).
18. O. Gonen, F. Arias-Mondoza, and G. Goelman, 3D localized *in vivo* ^{1}H spectroscopy of human brain by using a hybrid of 1D-Hadamard with 2D-chemical shift imaging, *Magn. Reson. Med.* **37,** 644–650 (1997).
19. O. Gonen, J. Hu, R. Stoyanova, J. S. Leigh, G. Goelman, and T. R. Brown, Hybrid three dimensional (1D-Hadamard, 2D-chemical shift imaging) phosphorus localized spectroscopy of phantom and human brain, *Magn. Reson. Med.* **33,** 300–308 (1995).
20. W. Dreher and D. Liebfritz, Double-echo multislice proton spectroscopic imaging using Hadamard slice encoding, *Magn. Reson. Med.* **31,** 596–600 (1994).
21. F. Delmas, B. Gillet, B.-T. Doan, J.-C. Beloeil, P. Meric, and J.-L. Correze, Proton localized 2D spectroscopy in the rat brain at 7T, Abstracts of the Society of Magnetic Resonance in Medicine, 8th Annual Meeting, Denver (2000), Abstract 1071.
22. P. A. Bottomley, Selective volume method for performing localized NMR spectroscopy, U.S. Patent 4,480,228 (1984).
23. H. Geen and R. Freeman, Band-selective radiofrequency pulses, *J. Magn. Reson.* **93,** 93–141 (1991).
24. J. Mao and T. H. Mareci, and E. R. Andrew, Experimental study of optimal selective 180° radiofrequency pulses, *J. Magn. Reson.* **79,** 1–10 (1988).
25. S. Müller, Multifrequency selective rf pulses for multislice MR imaging, *Magn. Reson. Med.* **6,** 364–371 (1988).
26. C. H. Cunningham and M. L. Wood, Method for improved multiband excitation profiles using Shinnar–Le Roux transform, *Magn. Reson. Med.* **42,** 577–584 (1999).
27. P. G. Webb, N. Sailasuta, S. J. Kohler, T. Raidey, R. A. Moats, and R. E. Hurd, Automated single-voxel proton MRS: Technical development and multisite verification, *Magn. Reson. Med.* **31,** 365–373 (1994).
28. D. A. Yablonskiy, J. J. Neil, M. E. Raichle, and J. J. H. Ackerman, Homonuclear J coupling effects in volume localized NMR spectroscopy: Pitfalls and solutions, *Magn. Reson. Med.* **39,** 169–178 (1998).
29. A. Ziegler, M. Izquierdo, C. Rémy, and M. Décorps, Optimization of homonuclear two-dimensional correlation methods for *in vivo* and *ex vivo* NMR, *J. Magn. Reson. B* **107,** 10–18 (1995).
30. R. Reddy, J. S. Leigh, and G. Goelman, Hadamard-spectroscopic-imaging-polarization-transfer technique, *J. Magn. Reson. B* **101,** 139–144 (1993).
31. M. Peres, O. Fedeli, B. Barrere, B. Gillet, G. Berenger, J. Seylaz, and J.-C. Beloeil, *In vivo* identification and monitoring of changes in rat brain glucose by two-dimensional shift-correlated ^{1}H NMR spectroscopy, *Magn. Reson. Med.* **27,** 356–361 (1992).
32. R. A. de Graaf, A. van Kranenburg, and K. Nicolay, Off-resonance magnetization transfer measurements on rat brain in situ, *Magn. Reson. Med.* **41,** 1136–1144 (1999).
33. K. L. Behar, T. Ogino, Assignment of resonances in the ^{1}H NMR spectrum of rat brain by two-dimensional shift correlated and *J*- resolved NMR spectroscopy, *Magn. Reson. Med.* **17,** 285–303 (1991).
34. S. Müller, Simultaneous multislice imaging (SIMUSIM) for improved cardiac imaging, *Magn. Reson. Med.* **10,** 145–155 (1989).